Journal XX (XXXX) XXXXXX

https://doi.org/XXXX/XXXX

# Propagating Dirac plasmon polaritons in topological insulators

# Yong Wang and Stephanie Law

Department of Materials Science and Engineering, University of Delaware, Newark, DE, 19716, USA

E-mail: slaw@udel.edu

Received xxxxxx Accepted for publication xxxxxx Published xxxxxx

#### **Abstract**

We investigate the excitation of propagating Dirac Plasmon Polaritons (DPPs) in topological insulator (TI) thin films. A series of TI thin films were grown by molecular beam epitaxy (MBE). Periodic gold grating couplers with different periodicity were fabricated on the TI films to excite the propagating DPPs. A series of absorption peaks that shift with the grating periodicity were observed in Fourier transform infrared spectroscopy (FTIR) transmission scans. We have ruled out any source other than the excitation of propagating DPPs that could have caused the peaks to appear. The peak dispersion is consistent with theoretical predictions for coupled DPPs in TI thin films.

Keywords: propagating Dirac plasmons, topological insulators, molecular beam epitaxy

#### 1. Introduction

The properties of topological insulators (TIs) have been widely explored due to their unique band structure, which comprises a bulk band gap crossed by surface states that form a Dirac cone [1-3]. TI surface states exhibit linear dispersion and spin-momentum locking in which the momentum of the particle determines its spin. Carriers occupying these surface states are therefore two-dimensional, massless, and spinpolarized [4]. Dirac plasmons can be excited from the carriers in the surface states. Since the thickness of TI thin films is much smaller than the wavelength of the incident light, plasmons excited on the top and bottom surfaces couple, resulting in an acoustic and an optical plasmon mode [5-6]. This article will focus on the excitation of the optical mode since this mode has a non-zero optical dipole moment and can be observed using Fourier transform infrared spectroscopy as described below. To date, localized optical coupled Dirac plasmon modes have been excited in TI films. By changing the film thickness and the wavevector of the localized Dirac plasmon, researchers have mapped out the dispersion relationship of these plasmons and have shown excellent agreement to theory [7-16]. In addition, localized TI Dirac plasmons show exceptionally large mode indices with relatively long lifetimes, making them promising for applications in terahertz sensing [17].

One of the unique features of propagating TI Dirac plasmons is their potential to carry spin. Because the TI Dirac carriers exhibit spin-momentum locking, a propagating plasmon excited from these carriers will comprise a spin density wave in addition to the charge density wave [18-20]. For propagating Dirac plasmons in a thin film, the coupled acoustic mode will have the spin waves in phase and the charge waves out of phase, while the coupled optical mode will have the spin waves out of phase and the charge waves in phase [19]. These excitations are of interest since no other single material system can support spin-polarized plasmons. The ability to use an optical pulse to launch a propagating spin plasmon could have applications in spintronics or in sensing of chiral molecules. It is currently unclear what the degree of spin polarization of this plasmon mode would be. Theoretical estimates for the degree of spin polarization of uncoupled TI electrons range from 0.5 to 0.6 [21], while experimental measurements range from 0.2-0.75 [22-25]. In order to

xxxx-xxxx/xx/xxxxxx 1 © xxxx IOP Publishing Ltd

understand the behavior of this propagating spin plasmon mode and determine the degree of spin polarization, we must first excite propagating Dirac plasmon polaritons (DPPs). Localized plasmon modes are essentially standing waves and do not have a non-equilibrium spin population. In this paper, we will excite DPP modes in a TI thin film using a gold grating rather than a localized geometry for the first time. We will map their dispersion and show that it matches theoretical predictions. This research lays the groundwork for probing the spin dynamics in propagating TI DPPs.

There have been previous successful efforts to excite Dirac plasmons in TI thin films. The most common way is to etch the film into an array of stripes to create localized plasmons [8-9]. Although this technique has been highly effective, these localized modes cannot easily be used to understand the spin properties of TI plasmons. To investigate propagating DPPs, we fabricated a metal grating coupler on top of an unpatterned TI thin film to excite our propagating plasmon, similar to what has previously been done in graphene [26-27]. The predicted dispersion relation for a single layer Dirac plasmon system such as graphene, shown in Eq. (1), indicates that the wavevector of the plasmon mode is much larger than light in free space.

$$\omega_{Dirac}^2 = \frac{e^2}{4\varepsilon_0\varepsilon_r} \frac{v_F\sqrt{2\pi n_D}}{h} q \tag{1}$$
 where  $\omega_{Dirac}$  is the plasmon frequency, q the wavevector,  $v_F$ 

the Fermi velocity, e is the charge on the electron,  $\varepsilon_0$  is the permittivity of free space,  $\varepsilon_r$  is the average permittivity of the materials above and below the TI, h is Planck's constant, and  $n_D$  is the density of the Dirac carriers [28-30]. To overcome this wavevector mismatch, we can use a metal grating coupler to match the momentum of light with that of the plasmon mode. When light travels into a grating coupler, a wavevector along the interface is created through diffraction. The grating wavevector is given by Eq. (2):

$$q_{grating} = \frac{2\pi}{\Lambda} \tag{2}$$

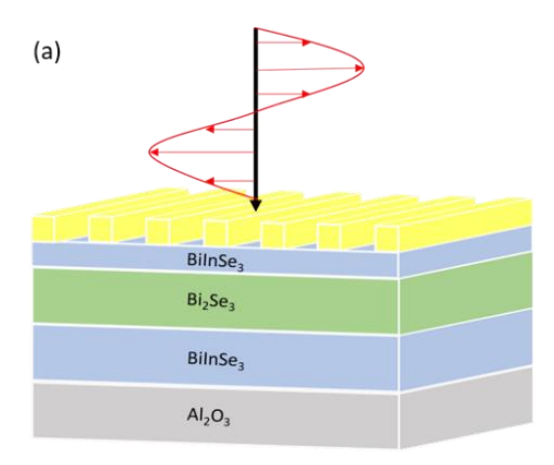
where  $\Lambda$  is the period of the grating coupler. This immediately leads us to the wavevector of the plasmon in Eq. (3):

$$q_{plasmon} = k_0 sin\theta + q_{qrating} \tag{3}$$

 $q_{plasmon} = k_0 sin\theta + q_{grating} \eqno(3)$  where  $q_{plasmon}$  is the wavevector of the plasmon,  $k_0$  the wavevector of the incident light,  $\theta$  the incident angle of the light.

#### 2. Experiments

We first grew a series of 50nm Bi<sub>2</sub>Se<sub>3</sub> films using a Veeco GenXplor molecular beam epitaxy system. The films had the following structure: a layer of 5nm BiInSe<sub>3</sub> (BIS) on the top, 50nm Bi<sub>2</sub>Se<sub>3</sub> TI in the middle, and 50nm BIS buffer layer between the TI and the (0001) Al<sub>2</sub>O<sub>3</sub> substrate as shown schematically in Fig. 1(a). The BIS layer on the top serves as a protective layer to prevent surface degradation and charge redistribution caused by the metal grating. The BIS layer on the bottom serves as a buffer layer to optimize the quality of the TI growth. For a detailed description of the growth procedure, readers are referred to our previous publications [31-33].



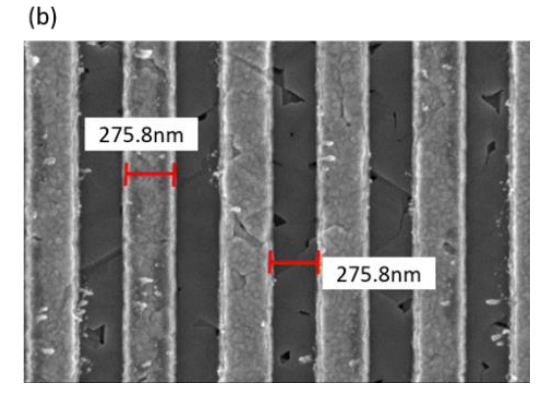


Fig. 1. (a) A schematic of a typical device and the geometry of the optical measurement. (b) A scanning electron microscope image for a typical sample with a grating with period 550nm.

After growth, 100nm gold/10nm titanium gratings with different grating periodicity are fabricated on the surface of film standard techniques using photolithography, electron beam lithography, electron beam deposition, and liftoff. The period of the gratings ranges from 400nm to 700nm. The width of the metal stripes was kept at 50% of the grating period for all samples. Fig. 1(b) shows an SEM image of a typical sample with a grating period of 550nm. After patterning, transverse magnetic (TM) polarized transmission spectra were taken using a Bruker Vertex 70v Fourier transform infrared spectroscopy (FTIR) system. For these experiments, TM-polarized spectra have the electric field of the incident light polarized perpendicular to the grating stripes as shown schematically in Fig. 1(a). Spectra were normalized to transmission through an unpatterned Al<sub>2</sub>O<sub>3</sub> substrate. As a control, TM transmission spectra were also taken on a bare Al<sub>2</sub>O<sub>3</sub> substrate fabricated with a gold grating with a period of 500nm, a single layer 50nm BIS film grown on Al<sub>2</sub>O<sub>3</sub> without a grating, and a multilayer film

without a grating. Fig. 1(a) shows the structure of a typical device. In the figure, the vertical arrow indicates the light with normal incidence. The curve and the horizontal arrows indicate the electric field of the light for TM polarization. In this case, the electric field is polarized perpendicular to the stripes.

#### 3. Results and Discussions

The TM extinction spectra for the samples with grating periods of 400nm, 450nm, 500nm, 550nm and 700nm are shown in Fig. 2(a). These samples are labeled A (black diamond), B (green up-triangle), C (blue circle), D (yellow square) and E (red hexagon), respectively. The extinction spectra were calculated by Eq. (4):

$$E = \frac{1 - \frac{T_S}{T_{Sub}}}{E_{\alpha}} \tag{4}$$

 $E = \frac{1 - \frac{T_S}{T_{sub}}}{E_{\alpha}}$  (4) where  $T_S$  is the transmission of the sample,  $T_{sub}$  is the transmission of the substrate, and  $E_{\alpha}$  is the extinction of the sample at the  $\alpha$ -phonon frequency. In order to make the plasmon absorption peak more obvious, we normalized the extinction spectra to the extinction of the  $\alpha$ -phonon peak. Since the gold gratings are covering half of the surface of the film, the extinction spectra are always above 0.5. This normalized extinction is plotted in Fig. 2(a).

In Fig. 2(a), we see a series of peaks shifting to lower frequencies as the grating periodicity increases. This behavior is consistent with expectations for Dirac plasmons: as the grating period increases, the wavevector decreases, which will cause the plasmon frequency to decrease. A zoomed in spectrum for all the sample in the range of 3-5THz can be found in Fig. 3(a).

Although our results are consistent with propagating DPPs, we must rule out any confounding effects. We therefore performed measurements on a series of control samples. These included a bare Al<sub>2</sub>O<sub>3</sub> substrate with 500nm grating (sample F), a 50nm BiInSe<sub>3</sub> film grown on Al<sub>2</sub>O<sub>3</sub> with no grating (sample G), and a complete multilayer film with no grating (sample H). The extinction spectra for samples F (gray lefttriangle), G (pink right-triangle) and H (black star) are shown in Fig. 2(b). For samples F and G, we do not observe any distinct peaks. For sample H, we see two peaks at ~2THz and ~4THz, which can be attributed to the  $\alpha$  and  $\beta$  phonons, respectively, in the multilayer sample. These phonon frequencies are fixed by the material and will not change with the grating period.

By comparing the extinction spectra for the samples shown in Fig. 2(a) with that of sample F, we can conclude that the absorption peaks in Fig. 2(a) do not arise from a pure grating coupler diffraction mode. If they did, we would expect to observe a peak in the extinction spectrum of sample F. The extinction spectra for samples G and H indicate that the absorption peaks that we observe in samples A-E above ~2THz are not from the bare materials alone, but are caused

by an interaction of light with the grating. Hence, a propagating plasmon mode would be the most probable explanation for the extra absorption peaks that we see in the terahertz range.

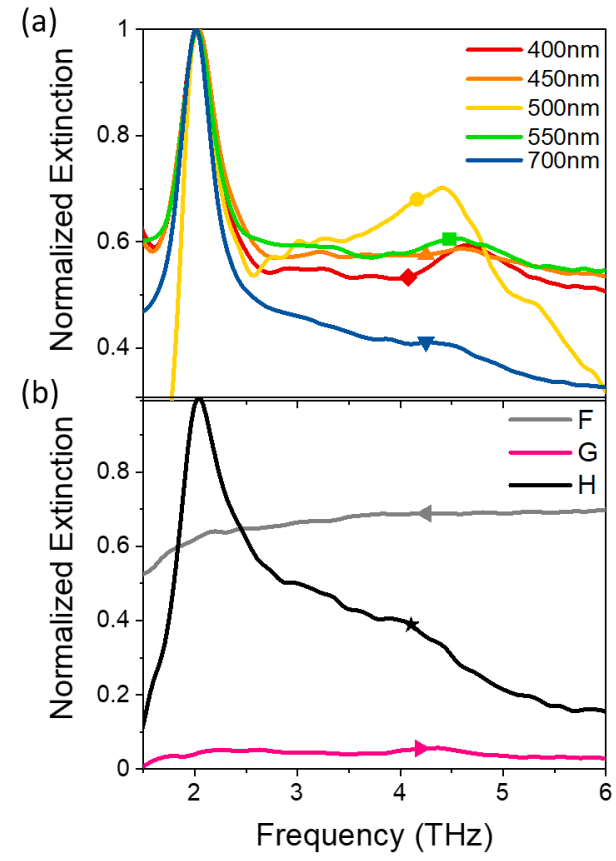


Fig. 2. (a) Normalized extinction spectra for the samples with grating periods as indicated in the legend. (b) Normalized extinction spectra for comparison samples: F, a bare Al<sub>2</sub>O<sub>3</sub> substrate with 500nm grating; G, a BIS layer without a grating; and H, a complete TI multilayer sample without a grating.

In order to be sure that these absorption peaks are caused by the excitation of DPPs, we need to plot the dispersion of the mode position. As there are no detailed models of the shape of a coupled propagating DPP mode, we chose the peak position by eye. In Fig. 3(a), we show a zoomed in version of the data plotted Fig. 2(a) over the 3-5THz range. The spectra are offset so that each sample can be distinguished easily. The arrows indicate the plasmon frequency for each spectrum that we use for our dispersion relation analysis. These extracted peak positions are plotted as colored symbols in Fig. 3(b). They are compared to the theoretical dispersion curve, shown as a black line.

The theoretical dispersion curve is generated from the dispersion relationship for the optical mode for coupled Dirac plasmons. Eq. (1) describes the dispersion for a Dirac plasmon

excited from a single surface, like graphene. In the case of a 50nm TI thin film, a coupling term that considers the contribution from both the top and bottom surfaces will be needed as shown by previous studies [7-8]. The coupled Dirac plasmon dispersion relation is shown in Eq. (5):

$$\omega_{Dirac}^2 = \frac{e^2}{\varepsilon_0} \frac{v_F \sqrt{2\pi n_D}}{h} \frac{q}{\varepsilon_T + \varepsilon_b + q\varepsilon_{TI}d}$$
 (5) where  $\varepsilon_T$  is the permittivity of the material on top of TI,  $\varepsilon_B$ 

the permittivity of the material below the TI,  $\varepsilon_{TI}$  is the permittivity of the TI material itself, and d is the thickness of TI thin film. For our TI films, the thickness d is 50nm, the Fermi velocity  $v_F = 5.0 \times 10^5 m/s$ , and the carrier density  $n_D = 1.4 \times 10^{13} cm^{-2}$  from room-temperature measurements [9]. The frequency-dependent permittivity of the TI thin film is generally well-known. However, the permittivity of the BIS material in the terahertz regime is less well-known; this material is found both above and below the TI. Because the BIS layers are much thinner than the wavelength of the terahertz light, it is likely that the excitation samples both the BIS permittivity as well as the permittivity of the Al<sub>2</sub>O<sub>3</sub> substrate and the permittivity of the air/gold grating. This adds an additional complexity in determining the effective permittivities above and below the TI thin film. In addition, we expect that the grating coupler will influence the effective permittivity of the material above the TI in an unknown way. Rather than guessing at the magnitude of these effects, we chose to use a constant value of the effective permittivity,  $\varepsilon_{eff}$ , as shown in Eq. (6):

$$\omega_{Dirac}^{2} = \frac{e^{2}}{\varepsilon_{0}} \frac{v_{F}\sqrt{2\pi n_{D}}}{h} \frac{q}{\varepsilon_{eff} + q\varepsilon_{TI}d}$$
(6)
Through the simulation, we found that the theory fits the

Through the simulation, we found that the theory fits the best with data at  $\varepsilon_{eff}=20.3$ , with a correlation value of 0.90. The simulation results with  $\varepsilon_{eff}=20.3$  are shown in Fig. 3(b) as a gray line, while the extracted resonance frequencies are shown as filled symbols. Each symbol represents the sample with the same color as shown in Figs. 2(a) and 3(a). Before we can be sure that these excitations are due to Dirac electrons, we must also rule out other sources of electrons. The TI thin films could have electrons in the bulk of the material caused by point defects during growth. They may also have a surface accumulation layer caused by band bending. In both of these cases, the electrons of interest are massive. The surface accumulation layer electrons are clearly two-dimensional and massive and will follow the 2D massive plasmon dispersion relationship shown in Eq. (7).

$$\omega_{massive}^2 = \frac{e^2}{4\varepsilon_0 \varepsilon_r} \frac{n_M}{m^*} q \tag{7}$$

where  $n_M$  is the density of the 2D massive electrons  $(1.4 \times 10^{13} cm^{-2})$  with an effective mass of  $m^*$   $(1.37 \times 10^{-31} \, kg)$ . In addition, because these films are much thinner than the wavelength of light, plasmons arising from massive carriers in the bulk of the film will also follow the 2D massive plasmon dispersion relationship shown in Eq. (7). To demonstrate that we are observing coupled Dirac plasmons

and not 2D massive plasmons resulting either from a massive surface accumulation layer or massive bulk carriers, we plotted the dispersion relation of 2D massive plasmons, shown as the gray dashed line in Fig. 3(b). We used  $\varepsilon_r = \frac{\varepsilon_{eff}}{2}$  as an approximation of the average permittivity of the materials surrounding the 2D electrons. It is clear that the plasmon modes we observe are not likely to be 2D massive plasmons, since the wavevectors of the 2D massive plasmons are orders of magnitude lower than that of the coupled Dirac plasmons. The density of the 2D massive carriers would need to be unrealistically high to get close to the experimental data. Finally, we can rule out the excitation of phonon polaritons, as calculations indicate that in the 3-5THz range, phonon polaritons would have wavevectors that are an order of magnitude smaller than these excitations. We therefore attribute our observations to the excitation of coupled propagating DPPs.

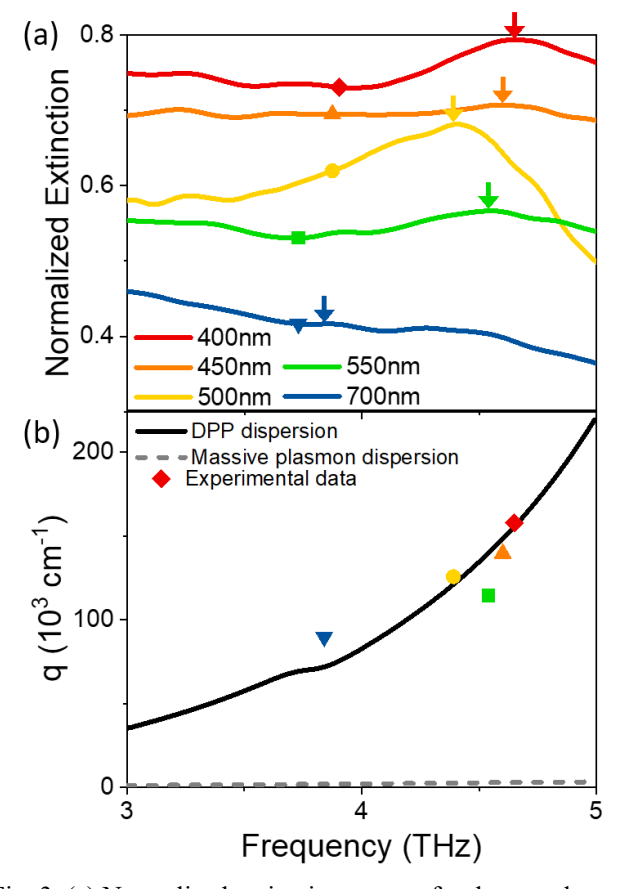


Fig. 3. (a) Normalized extinction spectra for the samples with different grating periods, zoomed in on the 3~5THz range with the extinction offset for clarity. (b) Theoretical dispersion of the coupled Dirac plasmon modes (black solid line) and 2D massive plasmon modes (gray dashed line). Symbols represent the experimental plasmon absorption peaks. The colors of the symbols are consistent with the spectra in (a).

We can see in Fig. 3(b) that the experimental resonant positions match the theoretical curve well. The sample with a 500nm grating width does deviate somewhat from the expected value. We do not believe this is caused by an incorrect grating period as these were all checked using scanning electron microscopy as shown in Fig. 1(b). Likewise, all of the TI thin films were grown as a batch; therefore, the film thickness should be the same in all cases. It is likely that this deviation is caused by measurement difficulties. The frequencies of the plasmons that we are exciting fall into the same range as the β phonon of Bi<sub>2</sub>Se<sub>3</sub> (~4THz); interactions between the plasmon and phonon make it somewhat more difficult to extract the plasmon peak position. This will be especially problematic as the grating period increases and moves the plasmon resonance closer to the  $\beta$  phonon frequency. In addition, the signal to noise ratio of the data is limited by the FTIR instrument in this frequency range, which also makes it difficult to determine the exact position of the peak. One way to mitigate this difficulty would be to try to excite the plasmons in a different frequency regime where the optical measurements are easier. However, shifting the plasmon frequency is challenging. According to the simulated dispersion relation of the DPP, we would need a grating with a smaller period (<400nm) to push the plasmon to higher frequencies, which is challenging in terms of device fabrication. The Al<sub>2</sub>O<sub>3</sub> substrates are also not transparent above ~8THz, so measurements at these frequencies would require shifting to a different substrate. Pushing the plasmon frequency lower to below the α phonon (~2THz) would cause measurement difficulties since the signal:noise ratio of the FTIR in this region is poor. Despite these difficulties, we are confident in our assignment of these excitations as propagating DPPs. This experiment lays the foundation for understanding and using the DPP in spintronic devices. In the future, we can move onto the direct detection of the correlated propagating spin wave by a THz-pump IR probe method using a magneto-optical Kerr effect (MOKE) system.

## 4. Conclusions

In conclusion, we grew a series of TI thin films in an MBE system, and then lifted off periodic gold grating couplers with different periodicities on top of the films. A series of peaks were observed in the FTIR extinction spectra. The absorption frequency decreased as the grating periodicity increased. We showed that these absorption peaks were not from the bare grating couplers or the bare materials. The dispersion of these peaks matched the theoretical dispersion curve for propagating DPPs. We therefore attribute these peaks to the excitation of DPPs in TI thin films using a gold grating. The success of this experiment will allow us to further investigate the unique spin properties of TI plasmons.

### **Acknowledgements**

Y. Wang and S. Law acknowledge the funding from the U.S. Department of Energy, Office of Science, Office of Basic Energy Sciences, under Award No. DE-SC0016380. We acknowledge the use of the Materials Growth Facility (MGF) at the University of Delaware, which is partially supported by the National Science Foundation Major Research Instrumentation Grant No. 1828141 and is a member of the Delaware Institute for Materials Research (DIMR).

### References

- [1] J. E. Moore 2010 Nature 464, 194
- [2] Y. L. Chen, J. G. Analytis, J.-H. Chu, Z. K. Liu, S.-K. Mo, X. L. Qi, H. J. Zhang, D. H. Lu, X. Dai, Z. Fang, S. C. Zhang, I. R. Fisher, Z. Hussain, and Z.-X. Shen 2009 Science 325, 178
- [3] M. Z. Hasan and C. L. Kane 2010 Rev. Mod. Phys. 82, 3045
- [4] R. Roy 2009 Phys. Rev. B 79, 195322
- [5] Y.-P. Lai, I.-T. Lin, K.-H. Wu, and J.-M. Liu 2014 Nanomater. Nanotechnol. 4, 13
- [6] S. D. Sarma, and E. H. Hwang 2009 Phys. Rev. Lett 102, 206412
- [7] T. Stauber, G. Gómez-Santos, and L. Brey 2017 ACS Photonics 4, 2978
- [8] P. Di Pietro, M. Ortolani, O. Limaj, A. Di Gaspare, V. Giliberti, F. Giorgianni, M. Brahlek, N. Bansal, N. Koirala, S. Oh, P. Calvani, and S. Lupi 2013 Nat. Nanotechnol. 8, 556
- [9] T. P. Ginley and S. Law, Adv. Opt. Mater. 6, 1800113(2018)
- [10] A. Karch 2011 Phys. Rev. B 83, 245432
- [11] M. Autore, F. D'Apuzzo, A. Di Gaspare, V. Giliberti, O. Limaj, P. Roy, M. Brahlek, N. Koirala, S. Oh, F. J. García de Abajo, and S. Lupi 2015 Adv. Opt. Mater. 3, 1257
- [12] M. Autore, H. Engelkamp, F. D'Apuzzo, A. Di Gaspare, P. D. Pietro, I. Lo Vecchio, M. Brahlek, N. Koirala, S. Oh, and S. Lupi 2015 ACS Photonics 2, 1231
- [13] M. Autore, P. Di Pietro, A. Di Gaspare, F. D'Apuzzo, F. Giorgianni, M. Brahlek, N. Koirala, S. Oh, and S. Lupi 2017 J. Phys. Condens. Matter 29, 183002
- [14] M. Autore, F. Giorgianni, F. D' Apuzzo, A. Di Gaspare, I. Lo Vecchio, M. Brahlek, N. Koirala, S. Oh, U. Schade, M. Ortolanic, and S. Lupi 2016 Nanoscale 8, 4667
- [15] A. Politano, V. M. Silkin, I. A. Nechaev, M. S. Vitiello, L. Viti, Z. S. Aliev, M. B. Babanly, G. Chiarello, P. M. Echenique, and E. V. Chulkov 2015 Phys. Rev. Lett. 115, 216802
- [16] C. In, S. Sim, B. Kim, H. Bae, H. Jung, W. Jang, M. Son, J. Moon, M. Salehi, S. Y. Seo, A. Soon, M. H. Ham, H. Lee, S. Oh, D. Kim, M.-H. Jo, and H. Choi 2018 Nano Lett 18, 734
- [17] I. Appelbaum, H. D. Drew, and M. S. Fuhrer 2011 Appl. Phys. Lett. 98, 023103
- [18] D.K. Efimkin, Yu. E. Lozovik, and A. A. Sokolik 2012 J. Magn. Mang. Mater. 324, 3610
- [19] S. Raghu, S. B. Chung, X.-L. Qi, and S.-C. Zhang 2010 Phys. Rev. Lett. 104, 116401
- [20] R. Schütky, C. Ertler, A. Trügler, and U. Hohenester 2013 Phys. Rev. B 88, 195311
- [21] O. V. Yazyev, J. E. Moore, and S. G. Louie 2010 Phys. Rev. Lett. 105, 266806

- [22] D. Hsieh, Y. Xia, D. Qian, L. Wray, J. H. Dil, F. Meier, J. Osterwalder, L. Patthey, J. G. Checkelsky, N. P. Ong, A. V. Fedorov, H. Lin, A. Bansil, D. Grauer, Y. S. Hor, R. J. Cava, and M. Z. Hasan 2009 Nature 460, 1101
- [23] Z.-H. Pan, E. Vescovo, A.V. Fedorov, D. Gardner, Y. S. Lee, S. Chu, G. D. Gu, and T. Valla 2011 Phys. Rev. Lett. 106, 257004
- [24] D. Hsieh, Y. Xia, L. Wray, D. Qian, A. Pal, J. H. Dil, J. Osterwalder, F. Meier, G. Bihlmayer, C. L. Kane, Y. S. Hor, R. J. Cava, and M. Z. Hasan 2009 Science 323, 919
- [25] S. Souma, K. Kosaka, T. Sato, M. Komatsu, A. Takayama, T. Takahashi, M. Kriener, K. Segawa, and Y. Ando 2011 Phys. Rev. Lett. 106, 216803
- [26] W. Gao, G. Shi, Z. Jin, J. Shu, Q. Zhang, R. Vajtai, P. M. Ajayan, J. Kono and Q. Xu 2013 Nano Lett. 13, 3698
- [27] L. Ju, B. Geng, J. Horng, C. Girit, M. Martin, Z. Hao, H. A. Bechtel, X. Liang, A. Zettl, Y. R. Shen, and F. Wang 2011 Nat. Nanotechnol. 6, 630
- [28] T. Stauber, and G. Gómez-Santos 2012 New J. Phys. 14, 105018
- [29] T. Stauber, and G. Gómez-Santos 2013 Phys. Rev. B 88, 205427
- [30] Y. Deshko, L. Krusin-Elbaum, V. Menon, A. Khanikaev, and J. Trevino 2016 Opt. Express 24, 7398
- [31] T. P. Ginley, and S. Law, J. Vac. Sci. Engr. B 2016 34, 02L105
- [32] T. P. Ginley, Y. Wang, and S. Law 2016 Crystals, 6, 154
- [33] Y. Wang and S. Law 2018 J. Vac. Sci. Engr. B 36, 02D101